A Method for Detection of Retinal Layers by Optical Coherence Tomography Image Segmentation

Ahmet M. Bagci, Rashid Ansari
Electrical and Computer Engineering Dept.
University of Illinois at Chicago
851 S Morgan St. Chicago, IL
abagci1@uic.edu, ansari@ece.uic.edu

Mahnaz Shahidi*
Dept. of Ophthalmology and Visual Sciences
University of Illinois at Chicago
1855 W Taylor St. Chicago, IL
mahnshah@uic.edu

***Abstract*— A novel algorithm is reported for automatically segmenting optical coherence tomography (OCT) images to identify six layers within the retina. The boundary detection technique presented here is based on a 2-D edge detection scheme, in which a filter with wedge-shaped pass band is introduced. The proposed filter enhances edges along the vertical boundaries while suppressing speckle noise. The detected contours are labeled based on a retina model. The layer thickness measurements derived by the algorithm are compared with thickness measurements from manually marked boundaries. The automated thickness measurements derived by the algorithm differ from manual segmentation results by less than 5 microns on average.**

I. INTRODUCTION

Thickness measurement of retinal layer is important as it provides useful information for detecting pathological changes and diagnosing retinal diseases. Optical coherence tomography (OCT) is an imaging modality that provides cross-sectional images of the retina, which makes it possible to measure retinal thickness. The commercially available OCT software only provides measurement of total retinal thickness, therefore limiting information on intraretinal structures.

Recently various approaches have been described for retinal thickness measurements from OCT images. Ishikawa et al. have described an approach to segment retinal layers and extract thickness of retinal layers [1]. The performance of this algorithm on StratusOCT images and ultrahigh resolution OCT images were compared and outer retinal complex thickness values were reported [2]. Koozekanani et al. described a method for extracting the upper and lower retinal boundaries with the use of a Markov model on OCT images [3]. Recently, a method based on an extension of Markov model was reported for analysis optic nerve head geometry [4]. Determination of retinal nerve fiber layer thickness based on a deformable spline (snake) algorithm has also been reported [5].

In this paper, we present a new algorithm to automatically detect six layers within the retinal tissue. Our method utilizes a filter that enhances edges along the image vertical dimension while suppressing speckle noise. The detected contours along the horizontal dimension are labeled based on a retina model. We report the average thickness of six retinal layers in 15 healthy subjects. Measurements obtained by the algorithm were compared to previously published three-layer automated segmentation findings [6] and manual segmentation results.

*This work was supported in part by the Dept of Veterans Affair.

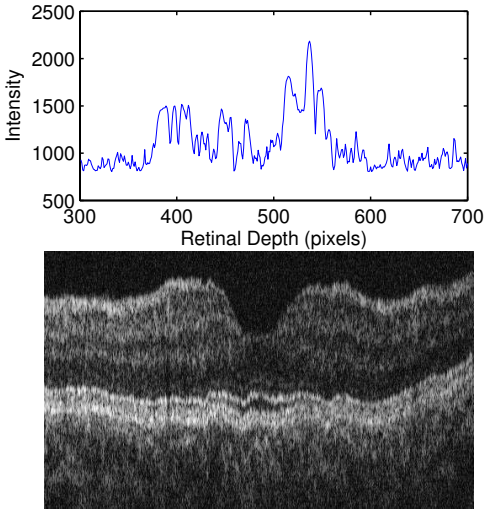

Fig. 1. (a) Sample A-scan. (b) Sample OCT image used in segmentation algorithm.

II. OCT INFORMATION AND RETINAL MODEL

A. OCT Image Information

The StratusOCT instrument generated time domain OCT images of the retinal tissue. The laser beam was scanned in retinal depth to generate an A-scan. Each cell layer within the retina tissue has different reflectance properties and produces peaks on the scan, a sample of which is shown in Fig. 1(a). A total of 512 A-scans are acquired from neighboring locations resulting in a cross sectional view, called a B-scan, a sample of which is shown in Fig. 1(b). Each column of a B-scan is composed of an A-scan.

Note that there are discontinuities and bumps in the OCT image, even though the actual retinal surface is generally smooth. These are partially due to involuntary eye motion, blurring retinal boundaries. Besides, there is considerable speckle noise in the image, which reduces the sharpness of

978-1-4244-1813-8/08/$25.00 ©

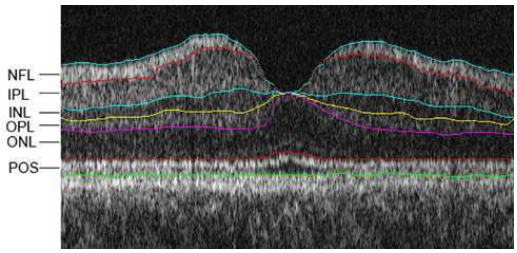

Fig. 2. Six layers are identified by the algorithm: nerve fiber layer (NFL) inner plexiform layer (IPL), inner nuclear layer (INL), outer plexiform layer (OPL), outer nuclear layer (ONL), photoreceptor outer segments (POS).

retinal boundaries. Both of these issues present a challenge for any algorithm that tries to detect continuous edges. Furthermore, the edge strength is not the same at different locations on the same layer boundary. Some other artifacts in the image such as blood vessels also need to be taken into account by the algorithm. It may be noted that the left hand side of the image usually appears somewhat brighter than the right hand side.

B. Retinal Layer Model

The algorithm identifies the following six layers in the image: nerve fiber layer (NFL) inner plexiform layer (IPL), inner nuclear layer (INL), outer plexiform layer (OPL), outer nuclear layer (ONL), photoreceptor outer segments (POS), as marked on the sample OCT scan shown in Fig. 2. The POS layer was bounded by the junction between the photoreceptor inner and outer segments (IS/OS) and the retinal pigment epithelium (RPE) inner boundary, bottom-most contour marked in Fig. 2. The algorithm uses the fact that the inner and outer plexiform layers appear brighter than inner and outer nuclear layers. In addition, the nerve fiber layer, RPE and junction between photoreceptor inner and outer segments appear brighter than the rest of the layers.

III. ALGORITHM DESCRIPTION

A. Outline of the Algorithm

The segmentation algorithm consists of the following steps:

- Alignment of A-scans.
- Gray-level mapping
- Directional filtering
- Edge detection
- Model based decision making

The details of each step are explained next.

B. Alignment of A-scans

It was noted in the previous section that one of the problems facing 2-D edge detection algorithms is that the columns of an OCT image are not necessarily aligned according to the physical location of the layer. In some of the earlier work on the topic, edge detection algorithms are implemented on each column individually to avoid complications to this misalignment of the individual A-scans [3]. In contrast we utilize the correlation between adjacent A-scans which increases effectiveness of the edge detection. The goal of this step is to identify a common reference point in each A-scan. Then each A-scan is shifted so that each of these reference points is at the same level as the neighboring column. These reference points are identified using a two-pass edge detection algorithm. At first the images are smoothed, using a Gaussian filter

$$G(x,y) = \frac{1}{2\pi\sigma^2} e^{-\frac{x^2+y^2}{2\sigma^2}} \tag{1}$$

where σ defines the rate of blurring on the image. Then we calculate the derivative of the image in the vertical direction using a filter with 2-D impulse response

$$L(x,y) = -\frac{x}{\pi\sigma^2} e^{-\frac{x^2+y^2}{2\sigma^2}} \tag{2}$$

Non-maximum suppression is used to obtain single pixel edges, and hysteresis thresholding is used to eliminate broken edges due to the operator fluctuating above and below a single threshold. This step in our method is similar to Canny edge detector [7].

The operation is repeated twice with different values of σ. The first pass provides heavy clutter suppression, while the second pass yields an accurate location. For the first pass we use $\sigma = 10$. This provides us with the two most prominent edges corresponding to the inner limiting membrane (ILM) and RPE. We choose to align the image according to the RPE boundary; therefore each A-scan is shifted vertically by the corresponding level. Due to heavy blurring to suppress noise, these locations are approximate. Therefore we perform a second pass for more accurate alignment where a smaller $\sigma = 3$ value is used. While a higher number of edges are marked on this pass, only the ones coinciding with the first pass are chosen. Then A-scans are shifted to their final position. Note that the blurring operations are only used to locate the RPE boundary initially, and do not change the pixel intensity values used in the following steps. The image shown in Fig. 1(b) is aligned using this algorithm and the output is shown in Fig. 2.

C. Gray-level Mapping

In OCT images the band between the RPE boundary and ILM contains primarily three brightness levels. The transitions between these layers produce edges with different strengths. For example a typical transition from NFL to ganglion cell layer represents a change in approximate gray level value from 1800 to 1100 (12-bit data), whereas a transition from OPL to ONL translates to a change in approximate gray level value from 1200 to 900. The second transition produces a weaker edge. To strengthen the weak edges we perform an adaptive gray-level mapping using

$$G_i(x,y) = \frac{1}{2}\left(1 + erf\left(\frac{f(x,y) - t_i}{\sqrt{2}\sigma_i^2}\right)\right) \tag{3}$$

where $f(x,y)$ is the input gray level, t_i is the reference level and σ_i controlled the slope of the mapping.

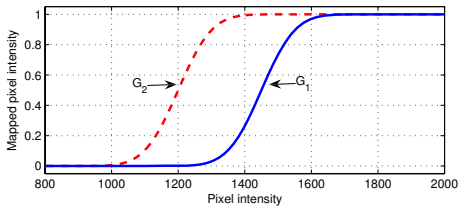

Fig. 3. Two gray level mapping functions with two different reference.

Two mapping functions were defined. The first mapping, G_1, is tuned for detection of boundaries between NFL and IPL+GCL and between IS/OS and RPE; the second mapping, G_2, is tuned for detection of boundaries between IPL, INL, OPL and ONL. Two parameters that define the mapping t_i and σ_i in (3) were decided adaptively for each OCT image using the expectation maximization (EM) algorithm [8]. The pixel values that lie within the ILM and RPE wee extracted and fed into the expectation maximization algorithm. We assumed that these pixel values contained three Gaussian mixtures. The maximum likelihood estimates for the mean and variance values of these mixtures were obtained using the EM algorithm, and used to set the optimal threshold values between these mixtures. These threshold values were used as the reference levels t_1 and t_2 in (3). The second parameter σ_i in (3) was decided using the variance values of the mixtures. The two mapping functions, G_1 and G_2, obtained for the image in Fig. 2 are plotted in Fig. 3. The rest of the operations in the algorithm were performed on these mapped intensity values individually; the boundary between NFL and IPL+GCL and the boundary between IS/OS and RPE was determined with G_1, while the remaining boundaries were determined with G_2.

D. Directional Filtering

Earlier we mentioned that one of the challenges in OCT images is the significant amount of noise that interferes with accurate edge detection. To overcome noise, Gaussian filtering is used in [6] and variants of median filtering are used in [3] and [1]. While they are effective in suppressing noise, these methods also tend to reduce edge sharpness.

To overcome edge blurring we employ a 2-D filter with a wedge-shaped pass band. This filter suppresses the speckle noise that produces high frequency variances in horizontal direction, while keeping the detail in vertical direction, which contains the boundaries of interest. The filter preserves edges lying within $\pm 45^\circ$ of the horizontal axis, which emphasizes the importance of the aligning columns so that the boundaries have a slope close to 0°. The frequency response of the filter is shown in Fig 4. The design of the filter, $F_h^{2v}(z_1, z_2)$, used here is based on our method used in [9]. The design is briefly described here for completeness. Design of $F_h^{2v}(z_1, z_2)$ starts with a special class of filters called the halfband filters. The 1-D halfband filter is expressed in the polyphase form as

$$H(z) = 1/2\left[1 + zP_1(z^2)\right] \tag{4}$$

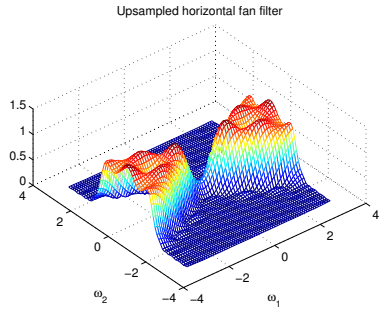

Fig. 4. Frequency response of the directional filter. The filter keeps the edges $\pm 45^\circ$ within the horizontal axis, while suppressing noise in other bands.

Based on $H(z)$, a square -passband 2-D low pass filter $L(z_1, z_2)$ is formed by,

$$L(z_1, z_2) = H(z_1)H(z_2) \tag{5}$$

A checkerboard filter $C_{13}(z_1, z_2)$ is obtained as the sum of two shifted versions of $L(z_1, z_2)$ as

$$\begin{aligned} C_{13}(z_1, z_2) &= L(jz_1, jz_2) + L(-jz_1, -jz_2) \\ &= 1/2[1 - z_1 z_2 P_1(-z_1^2)P_1(-z_2^2)] \end{aligned} \tag{6}$$

The fan filter transfer function is obtained by using the transformation

$$\begin{aligned} F_h(z_1, z_2) &= 1 - C_{13}(Z_1, Z_2)|_{Z_1 = z_1^{\frac{1}{2}} z_2^{\frac{1}{2}}, Z_2 = z_2^{\frac{1}{2}} z_1^{-\frac{1}{2}}} \\ &= 1/2[1 + z_2 P_1(-z_1 z_2)P_1(-z_1^{-1} z_2)] \end{aligned} \tag{7}$$

Finally the fan filter is upsampled vertically to obtain

$$F_h^{2v}(z_1, z_2) = F_h(z_1^2, z_2) \tag{8}$$

The design of directional filter banks is discussed in detail in [9].

E. Edge Detection

In this step we obtain the candidate contours for boundaries. An edge detection kernel based on the first derivative of Gaussian in vertical direction is used, as described in (9):

$$L(x, y) = -p\frac{x}{\pi\sigma^2} e^{-\frac{x^2+y^2}{2\sigma^2}} \tag{9}$$

We obtain satisfactory results with $\sigma = 3$. The parameter p determines the polarity of the edges, and takes values either 1 or -1. The edge detection kernel is applied twice with alternating values of p on the output of directional filtering. The peak values are marked as edges, using non-maximum suppression and hysteresis thresholding as described in section III-B. The boundaries between each pair of adjacent bright and dark regions, with bright on top, such as NFL-GCL, IPL-INL, and OPL-ONL, are extracted with $p = 1$ while rest of the boundaries are extracted with $p = -1$. At the output of this step, major significant contour segments and their polarities are marked. The output is usually not a continuous stretch of a contour from the left end of the image to the right, but it consists of contour segments with gaps. The gaps between segments are filled in the next step.

TABLE I

SEGMENTATION RMSE AND STANDARD DEVIATION VALUES IN PIXELS

Inner Bnd.	NFL	IPL	INL	OPL	ONL	IS/OS	RPE
RSME	3.3	5.0	4.3	4.4	5.5	3.5	2.6
Std. Dev.	0.4	1.6	1.4	1.5	1.7	0.6	1.1

F. Model Based Decision Making

The classification and labeling of edges and creation of continuous contours are performed in this step. The marking of the boundaries of the inner limiting membrane (ILM) and RPE in the first step were found to be robust. These boundaries are therefore used to serve as reference points. We use a model that contains the approximate location of each boundary. In this model, for each column in the image, the location of each boundary relative to ILM is stored as a ratio

$$l_i = \frac{d_i - d_1}{d_7 - d_1} \tag{10}$$

where d_1 refers to the pixel location of the ILM, d_7 refers to RPE, and for $i = 2, .., 6$, d_i refers to the location of the boundaries within the retina from top to bottom, as described earlier. For any column in the image, starting from the top we expect to see boundaries between NFL, IPL, INL, OPL, ONL, which correspond to edges with the polarities $(+1, +1, -1, +1)$ in this order. If this order is exactly satisfied, each of these contours are tentatively labeled and the actual ratio l_i^* for each of these boundaries in the column are calculated

$$l_i^* = \frac{d_i^* - d_1^*}{d_7^* - d_1^*} \tag{11}$$

where d_i^* refers to the actual location of the detected contour. Then the detected edge location is compared with the preset model and if $(l_{i-1} + l_i)/2 < l_i^* < (l_{i+1} + l_i)/2$ is satisfied, then the contour containing the point d_i^* is selected and labeled. This method works well for strong edges, but occasionally some clutter is also marked as a boundary pixel. These false positives appear as discontinuities along the boundary and removed using a simple median filter.

Finally we need to fill in the gaps along the boundary where there are insufficient edge clues. At this point, the model is fine tuned using the edge clues that were already labeled, and the gaps along the boundary are filled in according to the updated model.

IV. EXPERIMENTAL RESULTS

To test the validity of our algorithm, we performed automated segmentation on OCT images acquired in 15 healthy subjects. Six radial scans per subject were acquired. Each OCT scan was 512 pixels (6 mm) in length (horizontal dimension) and 1024 pixels (2 mm) in depth (vertical dimension). The intensity value of each pixel ranges between 700 and 2400. The vertical (scan 1 of 6) and horizontal (scan 4 of 6) OCT scans were also manually segmented by an observer. The average root mean squared error values (RMSE) and standard deviation for each layer between the manual marked inner boundaries and automatically marked inner boundaries are presented in Table I in pixels. The RMSE for detection of boundaries ranged between 2.6 and 5.5 pixels, corresponding to 5.2 and 11.0 microns.

TABLE II

THICKNESS AND STANDARD DEVIATION OF THE LAYERS BY MANUAL AND AUTOMATED SEGMENTATION

Layer	NFL	IPL	INL	OPL	ONL	POS
Manual (μm)	31.0	68.5	29.9	32.3	77.2	36.7
Std. Dev.	4.3	8.3	2.7	3.9	6.2	2.9
Expert (μm)	29.0	69.8	28.8	33.2	78.0	29.1
Std. Dev	6.5	14.8	4.0	5.8	7.1	3.4

The average thickness and standard deviation of retinal layers are reported in Table II. The average difference between automated and manual segmentation was less than 5 microns. The inner retina (NFL+IPL+INL+OPL), and ONL thickness measured by our method (162 ± 19 and 77 ± 6 μm) are consistent with previously reported thickness values (170 ± 39 and 78 ± 10 μm)[6].

V. CONCLUSIONS

In this paper we present a new algorithm to automatically detect six layers within the retina tissue. We report segmentation results that are consistent with manual segmentation. We established average thickness for the six retinal layers in 15 healthy subjects. In the future, we plan to apply our algorithm to higher resolution spectral domain OCT images and investigate changes in thickness of retinal layers in due to disease.

REFERENCES

[1] H. Ishikawa, D.M. Stein, G. Wollstein, S. Beaton, J.G. Fujimoto, and J.S. Schuman. Macular segmentation with optical coherence tomography. *Invest Ophthalmol Vis Sci*, 46:2012–2017, Jun 2005.

[2] A. Chan, J.S. Duker, H. Ishikawa, T. Ko, J. Schuman, and J. Fujimoto. Quantification of photoreceptor layer thickness in normal eyes using optical coherence tomography. *Retina, The Journal Of Retinal And Vitreous Diseases*, 26:655–660, 2006.

[3] D. Koozekanani, K. Boyer, and C. Roberts. Retinal thickness measurements from optical coherence tomography using a markov boundary model. *IEEE Transactions on Medical Imaging*, 20:900–916, September 2001.

[4] K. Boyer, A. Herzog, and C. Roberts. Automatic recovery of the optic nervehead geometry in optical coherence tomography. *IEEE Transactions On Medical Imaging*, 25:553–570, May 2006.

[5] M. Mujat, R. Chan, B. Cense, B. Park, C. Joo, T. Akkin, T. Chen, and J. de Boer. Retinal nerve fiber layer thickness map determined from optical coherence tomography images. *Optics Express*, 13:9480–9491, November 2005.

[6] M. Shahidi, Z. Wang, and R. Zelkha. Quantitative thickness measurement of retinal layers imaged by optical coherence tomography. *Am J Ophthalmol*, 139:1056–1061, June 2005.

[7] J. Canny. A computational approach to edge detection. *IEEE TransactionsPattern Anal. Mach. Intell*, 8:679–698, November 1986.

[8] A. Dempster, N. Laird, and D. Rubin. Maximum likelihood from incomplete data via the em algorithm. *Journal of the Royal Statistical Society, Series B*, 39:1–38, 1977.

[9] A.M. Bagci, R. Ansari, and W. Reynolds. Low-complexity implementation of non-subsampled directional filter banks using polyphase representations and generalized separable processing. *Electro/Information Technology Conference 2007*, pages 471–476, May 2007.